Appl Phys B (2012) 107:1031–1042
DOI 10.1007/s00340-011-4824-5

Applied Physics B
Lasers and Optics

A quantum sensor for high-performance mass spectrometry

D. Rodríguez

Received: 16 May 2011 / Revised version: 30 August 2011 / Published online: 26 November 2011

Abstract A novel device, called quantum sensor, has been conceived to measure the mass of a single ion with ultimate accuracy and unprecedented sensitivity while the ion is stored and cooled in a trap. The quantum sensor consists of a single calcium ion as sensor, which is laser cooled to mK temperatures and stored in a second trap connected to the trap for the ion under study by a common endcap. The cyclotron motion of the ion under investigation is transformed into axial motion along the magnetic field lines and coupled to the sensor ion by the image current induced in the common endcap. The axial motion of the sensor ion in turn is monitored spatially resolved by its fluorescence light. In this way the detection of phonons can be upgraded to a detection of photons. This device will allow one to overcome recent limitations in high-precision mass spectrometry.

1 Introduction: physics motivation

Mass spectrometry is one of the most important, essential and basic techniques in modern science. This is because the mass of a fundamental particle is a fundamental property of the particle itself, or, in a composite quantum mechanical system such as an atom, the mass is the sum of the masses of all its building blocks minus the binding energy between those constituents. The binding energy, which can be determined by measuring the mass of the composite system as well as those of its building blocks, reflects all physical forces acting in such a quantum system: These are the strong, electromagnetic and weak forces.

D. Rodríguez (✉)
Departamento de Física Atómica Molecular y Nuclear,
Universidad de Granada, 18071, Granada, Spain
e-mail: danielrodriguez@ugr.es
Fax: +34-958249487

High-precision mass spectrometry by means of Penning traps is a very active field of research at radioactive beam facilities as well as university laboratories (see e.g. [1, 2]). The current applied techniques, however, do enable to access especial and very attractive physics cases which require a mass spectrometer of highest performance. Example of these cases are: (a) the determination of the nuclear masses and in this way of the binding energies of superheavy elements in order to test nuclear theories in extreme conditions and to assign the proton number Z to the isotopes and superheavy elements synthesized by hot fusion, and (b) accurate measurement of the Q_β-value of the decay of $^{187}\mathrm{Re} \rightarrow {}^{187}\mathrm{Os}$ for a determination of the mass of the electron antineutrino as aimed at by the MARE I campaign.

1.1 The masses of superheavy elements

Superheavy elements (SHEs) are exotic quantum mechanical systems made of large numbers of protons and neutrons which owe their stability due to subtle contributions by pairing and shell effects to the binding energy. Production, existence, half-life and decay properties depend very critically on this energy and have therefore to be determined with high accuracy. Once experimentally known, these results provide stringent tests for nuclear models and mass formulas which in turn predict the location of proton and neutron shell closures. A number of nuclear models predict a so-called island of stability at the magic numbers $Z \approx 120$ and $N \approx 184$ whereby the exact Z for the shell closure is unsure [3].

SHEs are produced in fusion reactions and are connected in some cases by α-chains to the backbone of known isotopes, or one element in this decay chain might decay by fission (see e.g. Refs. [4–7]). In the latter case a link is missing to the backbone of known isotopes and elements, and the proton number of these isotopes cannot be unambiguously

identified. Accurate mass measurements of these elements will provide stringent arguments for a correct assignment of the superheavy elements to an atomic number Z. For this purpose, an absolute mass accuracy of the order of some 10 keV is sufficient. This corresponds to a relative uncertainty of 10^{-7} now in reach by state-of-the-art mass spectrometry using Penning traps.

Up to very recently, direct mass measurements were limited to isotopes of elements not heavier than uranium. A breakthrough was the measurement of the nobelium ($Z = 102$) isotopes ^{252,253,254}No produced with cross sections of 2 μb (≈ 2 ions/s), 1 μb (≈ 1 ion/s) and 0.5 μb (≈ 0.5 ions/s), respectively, performed by the SHIPTRAP Collaboration at the heavy ion accelerator UNILAC and the velocity filter SHIP at GSI in Darmstadt, [8]. The mass uncertainties range from 13 keV for ^{253}No to 31 keV for ^{252}No [9]. These results represent the very first direct mass measurement above uranium and improve the knowledge of many masses of neighboring isotopes up to darmstadtium ($Z = 110$) due to a manifold of links. Subsequent mass measurements on the $Z = 103$ isotope ^{256}Lr, produced with a rate of 1–2 ions per minute, sets basically the limit of the time-of-flight (TOF) technique [1, 10] currently in use. The extremely low production rate for superheavy nuclei ranging from about 1 to 10 pb (one ion per few days) for $114 \leq Z \leq 118$ [7, 11], is a real hurdle which can be overcome by a completely new approach.

1.2 The mass of the electron antineutrino

The observation of neutrino oscillations implies a non-zero neutrino mass ($m(\nu_e) \neq 0$) [12]. So far, the experiments aiming at directly measuring the mass of the electron antineutrino only succeeded to set an upper limit. The present limit of this mass is $m(\nu_e) < 2$ eV (at 95% C.L.) [13]. This number is the outcome of the analysis of two experiments, one in Troitsk [14], and the other at the University of Mainz [15]. They investigated the tritium β-decay using electrostatic retardation spectrometers and analyzed the energy region near the endpoint energy of the β-decay spectrum [13].

There are at present in the world two large collaborations working to improve the accuracy in the determination of the mass of the electron antineutrino: the KArlsruhe TRItium Neutrino experiment (KATRIN) and the Micro-calorimeter Array for a Rhenium Experiment (MARE). KATRIN is in the final stage of construction to continue studying the β-decay spectrum of tritium ($T_{1/2} = 12.3$ y, $E_0 = 18.5$ keV) using a larger electrostatic retardation spectrometer as compared to the one used at Mainz. It is aiming at improving the limit by an order of magnitude to ≤ 0.2 eV (see e.g. Ref. [16]). MARE is conceived to study the decay of ^{187}Re ($T_{1/2} = 41.2 \times 10^9$ y, $E_0 = 2.5$ keV) [17] using cryogenic calorimeters. The lower Q-value compared to KATRIN is an advantage in order to achieve a similar accuracy as KATRIN. Preceding experiments to MARE were MANU [17] and MIBETA [18]. The former yielded an upper limit of $m(\nu_e) < 26$ eV using a crystal of 1.5 mg of metallic rhenium cooled down to 60 mK with an activity of 1 Bq. The second approach consisted of an array of 10 $AgReO_4$ crystals, each 300 μg, which has resulted in $m(\nu_e) \leq 15$ eV. With further improvements planned, MARE will be realized in two steps: MARE I aims at an accuracy of 2 eV and the goal of MARE II is 0.2 eV [19, 20].

Mass measurements of the pairs ^{3}H–^{3}He and ^{187}Re–^{187}Os play an important role because they provide stringent constraints. The direct mass determination of the electron antineutrino in the KATRIN and in the MARE experiment relies on a very accurate determination of the shape of the β-spectrum near the endpoint where it is sensitive to the neutrino mass. Setting the neutrino mass to zero and extrapolating the β-spectrum to zero intensity, the extrapolated endpoint energy must coincide with the Q-value determined by mass spectrometry. In the case of ^{187}Re and ^{187}Os, masses have to be measured using a new approach in order to achieve the accuracy needed for the proposed investigations.

2 Present status in Penning trap mass spectrometry

The Penning trap is the most suitable and most advanced device to perform high-precision mass measurements. In this device the ions are confined by the combination of a strong homogeneous magnetic field, provided by a superconducting solenoid, and a quadrupole electrostatic field [1, 21]. The electric field is originated by applying DC potentials to one ring and two endcap electrodes made with hyperbolical shapes as shown schematically in Fig. 1. In order to confine particles with positive polarity, the potential difference between endcaps and ring electrode (U in Fig. 1) must be positive. The motion of the ion in a Penning trap can be described as the superposition of three independent motions,

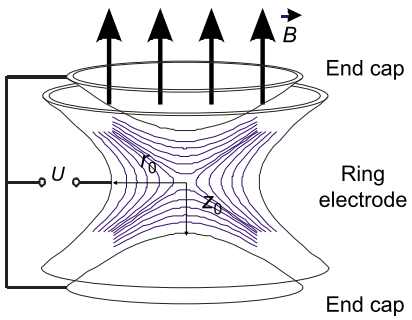

Fig. 1 Sketch of the hyperbolical Penning trap. Equipotential lines are indicated which are hyperboloids of revolution

one in the axial direction, and two in the radial plane. The axial motion has a characteristic frequency

$$\nu_z = \frac{1}{2\pi}\sqrt{\frac{qU}{md^2}}, \tag{1}$$

where m is the mass of the ion, q the electric charge, and d a parameter which describes trap dimensions by

$$d = \sqrt{\frac{z_0^2}{2} + \frac{r_0^2}{4}}. \tag{2}$$

The motions in the radial plane, named as modified-cyclotron and magnetron, respectively, have the characteristic frequencies

$$\nu_\pm = \frac{\nu_c}{2} \pm \sqrt{\frac{\nu_c^2}{4} - \frac{\nu_z^2}{2}}, \tag{3}$$

where ν_c is the cyclotron frequency of an ion moving in a magnetic field with strength B. The cyclotron frequency is related to the mass-to-charge ratio of the ion by

$$\nu_c = \frac{1}{2\pi}\frac{q}{m}B. \tag{4}$$

In the ideal Penning trap one finds

$$\nu_c = \nu_+ + \nu_-, \tag{5}$$

while in the real Penning trap and, for very precise cyclotron frequencies determinations ($\delta\nu_c \leq 10^{-9}$), the invariance theorem holds [21] given by

$$\nu_c^2 = \nu_+^2 + \nu_-^2 + \nu_z^2. \tag{6}$$

The mass of the trapped ion is determined from the cyclotron frequency which is obtained from the characteristics frequencies using (5) or (6). Two techniques are currently applied [1]:

- Detection by the time-of-flight technique (TOF technique). This technique is destructive and requires at least several tens of detected ions.
- Detection by image currents induced by the orbiting ion in the trap electrodes. This technique is non-destructive and a single ion is sufficient to perform a mass determination at cryogenic temperature.

The TOF technique determines the mass of an ion by measuring the time required by an ion, ejected out of the Penning trap, to reach an ion detector placed outside the magnetic field of the superconducting magnet [22]. This TOF is measured as a function of the applied radiofrequency (ν_{RF}). About 50–100 ejected ions have to be observed in order to create a spectrum with sufficient statistics. The application of this technique to SHEs is completely out of question, since the production cross sections drop to ≈ 10 pb, corresponding to about 1 ion produced per 2 days as recently observed at GSI [7]. The TOF technique can neither be applied to study the decay $^{187}\mathrm{Re} \rightarrow {}^{187}\mathrm{Os}$, since it can provide mass determinations with relative uncertainties ranging commonly from 10^{-7} to 10^{-9}, and in exceptional cases (when dealing with highly charged ions) down to 10^{-10}, which still is not sufficient.

With the second method and using the endcaps for detection, the current induced by one ion can be written as

$$I_{\mathrm{induced}} = 0.8 \cdot q \cdot \frac{2\pi\nu_z z}{2z_0}, \tag{7}$$

where $2z_0$ is the distance between the endcaps (Fig. 1) and z is the displacement of the ion in the axial direction from the trap center. The factor 0.8 accounts for the hyperbolical shapes of the endcaps. Since this current is small ($\approx$ fA), amplification is required but this will also increase the signal due to electronic noise. At room temperature, at least 100 ions must be stored simultaneously in the trap in order to obtain a signal above noise level. This technique is referred to as Fourier Transform Ion Cyclotron Resonance (FT-ICR) or Fourier Transform Mass Spectrometry (FT-MS) [23, 24]. It is also excluded for mass measurements of superheavy elements due to the extremely low production rate and of the pair ^{187}Re–^{187}Os because of the required accuracy: already two ions stored in the trap generate frequency shifts due to their Coulomb interaction. Therefore, either because of yield or because of accuracy, the mass measurements addressed in this publication must be carried out using one ion at a time in the trap.

There are worldwide two Penning trap mass spectrometers in operation which are designed to measure the mass of a single stable isotope with ultimate accuracy: the one developed at the University of Washington (UW-PTMS) by Van Dyck et al. [25], now at the Max-Planck Institute for Nuclear Physics in Heidelberg in the division of Blaum [26], and the one developed at MIT by Pritchard et al. [27] which was relocated in 2004 at FSU in Florida and is now operated with on-going success by the group of Myers [28].

Using the UW-PTMS, an uncertainty of 10 ppt has been accomplished for $^{16}\mathrm{O}^{6+}$ [25]. The MIT group even reported frequency ratio with an uncertainty of 7 ppt on the doublet CH^+–N^+ [27]. Both mass spectrometers operate at the temperature of liquid helium and apply resistive cooling, though the mass of the single ion is obtained using different strategies. The group at the University of Washington measured the cyclotron frequency of the ion of interest and the reference ion sequentially. The determination of ν_+ is carried out by observing a shift in the axial frequency ν_z. The MIT group developed a technique, which they called ion balance, using two ions simultaneously stored in the trap. The group at FSU uses the same spectrometer and two ions simultaneously stored in the trap but a technique previously developed

by Gabrielse et al. [29]. ν_+ is determined by measuring the cyclotron phase versus time using the so-called PNP (Pulse aNd Phase) technique (for more details see Refs. [30–32]).

There are two possibilities to detect the induced image current, either using a tuned LC circuit [33], or a tuned superconducting quantum interference device (SQUID) [34] in resonance with the trapped ion. Resonance means that the oscillation frequency of the trapped ion to be measured must be identical to the one of the equivalent circuit consisting of an inductance L from the coil and a capacitance C due to the electrodes. If the axial motion of the ion is in resonance with the LC circuit, $2\pi\nu_z = 1/\sqrt{LC}$, an amplification is obtained. This amplification is represented by the so-called $\widetilde{Q}$-value yielding an effective impedance $Z = \widetilde{Q}/(2\pi\nu C)$. The voltage signal S is the product $I_{\text{induced}} \cdot Z$, with I_{induced} as given in (7). The signal-to-noise ratio is given by

$$\frac{S}{N} = 0.8\sqrt{\pi} \cdot q \cdot \sqrt{\frac{\nu_z}{\Delta\nu}} \cdot \sqrt{\frac{\widetilde{Q}}{2k_B T C}} \cdot \left(\frac{z}{2z_0}\right), \tag{8}$$

where k_B is the Boltzmann constant, $\Delta\nu$ the spectral bandwidth, and T the temperature of the circuit, all these factors coming from the Johnson noise N. For a tank circuit cooled by liquid helium, the final temperature of the ion in the trap will be 4 K. As in (7), z is the axial oscillation amplitude. Using a single ion in a Penning trap, the maximum value of z/z_0 and therefore the maximum axial energy of the ion is limited, either by the size of the trap, or, if high-accuracy must be reached, by the maximum tolerable inhomogeneities and imperfections of the field the ion can feel when moving out of the trap center. Since the cyclotron motion will be detected through the induced image current in the endcap electrodes after conversion to axial motion, it is important to find a detection technique which allows reducing the radius of the cyclotron orbit and thus the axial oscillation amplitude.

3 The quantum sensor: a new concept in mass spectrometry

The quantum sensor will allow to overcome the current limitations in mass spectrometry by reducing considerably the ratio z/z_0. A kind of quantum sensor was discussed theoretically by Heinzen and Wineland 20 years ago [35] but has not been realized up to now. It is a novel technique for cooling, detection and mass spectrometry of a single ion. The basic idea is to separate functions and to make the action of radiofrequency detectable in the optical regime: By using laser spectroscopic detection instead of electronic detection of image charges, the sensitivity will be enhanced and frequency shifts minimized.

The mass measurement takes place using a system consisting of two adjacent traps in the same homogeneous region of the superconducting solenoid: the measurement trap confining the ion of interest for which the mass should be determined and the sensor trap which confines a sensor ion suited for laser cooling. $^{40}Ca^+$ will be used as sensor ion (this will be discussed in more detail in Sect. 4). The measurement procedure consists of six steps shown sequentially in Fig. 2:

1. The sensor ion is laser cooled to the Doppler limit ($T_{\text{limit}} \approx 80$ μK). This corresponds to a kinetic energy of 10 neV which is approximately 25 quanta of energy ($h\nu_z$). The cooling can be monitored either by a CCD camera or by a photomultiplier. The cooling time for the ion to reach the Doppler limit is in the order of millisecond. The ion under investigation and the sensor ion are not coupled.
2. The ion of interest is injected parallel to the magnetic field lines and captured in the first trap. The traps remain uncoupled and there is no damping on the motion of the ion of interest.
3. The two ions are coupled via the common endcap and by making their axial frequencies equal. This can be achieved by tuning the DC potential applied to the ring electrode with the endcaps connected to ground. The common endcap is connected to ground through a large resistor R when the axial motions of the two ions are coupled in order to cool the ion of interest. Side-band coupling will cool the radial motion.
4. The cyclotron motion of the ion of interest is excited by applying an external radiofrequency field (ν_{RF}) while the two ions are not coupled. Applying a quadrupole field at $\nu_{RF} = \nu_c$ [22] or a dipole field at $\nu_{RF} = \nu_+$ [25] results in an energy gain and an increase of the cyclotron radius (r_+).
5. The cyclotron motion is converted into axial motion by a π-pulse and the two ions are coupled. The laser is OFF so that there is an energy transfer from the ion of interest to the sensor ion.
6. After energy transfer, the laser is ON again. The time to achieve maximum fluorescence is recorded.

The measurement procedure is repeated for different radiofrequencies ν_{RF}, either around ν_c, or around ν_+. The feasibility of this method lies on the coupling of the ion of interest and the sensor ion, and thereafter on the cooling of the sensor ion using the laser beam.

3.1 Coupling the ion of interest and the sensor ion by image currents

The two traps sketched in Fig. 2, and by this the two ions, are coupled by tuning the axial frequency of the investigated ion

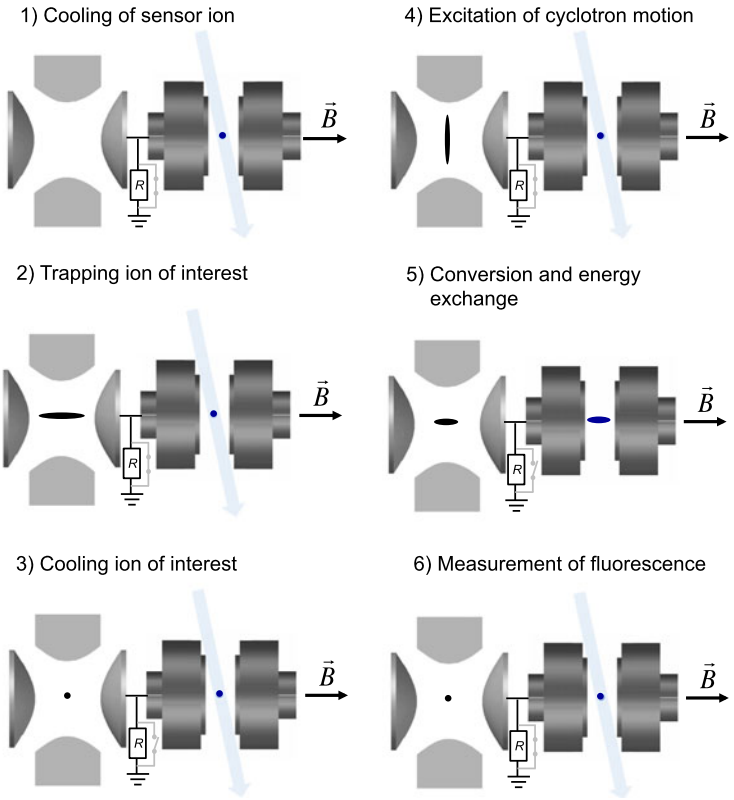

Fig. 2 Measurement sequence for the quantum sensor: The ion of interest is stored in the trap on the *left*, while the sensor ion is stored in the one on the *right*. The laser beam is represented by the *light-blue arrow* (color version): (**1**) The sensor ion is laser cooled to sub-mK temperatures; (**2**) the ion of interest is injected into the measurement trap; (**3**) the axial motion of the ion of interest is coupled to the sensor ion and cooled; (**4**) a radiofrequency field at $\nu_{RF} = \nu_c$ or $\nu_{RF} = \nu_+$ is applied to the ion of interest to excite the cyclotron motion; (**5**) the radial motion of the ion of interest is converted into axial motion and the laser beam is blocked so that energy exchange takes place between the two ions; (**6**) the laser is on again to observe the fluorescence. A switch (indicated in *light grey color*) is connected in parallel to a resistor with large resistance R. It will be closed while the ions are not coupled and open when they are coupled after tuning their axial oscillation frequencies. In such a way the endcaps are connected to ground through the resistor in order to minimize the current flowing to ground

to that of the sensor ion. In order to avoid the current flowing to ground, the resistor R must be larger than the impedance $Z = 1/(2\pi\nu_z)C$, with C being the total capacitance which is the sum of the capacitance of the central endcap electrode to all other electrodes and to the shield. Considering an axial frequency of $\nu_z = 100$ kHz and a capacitance $C = 1$ pF, the impedance results in 1.6 MΩ. For these conditions, a resistor with large resistance $R \approx 100$ MΩ (available in small chips), might be used. The time constant of the resulting RC-circuit is 100 µs, which is a factor of 10 larger than the axial oscillation period at $\nu_z = 100$ kHz.

Cooling is accomplished by laser cooling the sensor ion after the axial frequencies for the investigated ion and the sensor one are identical. This will take several seconds according to [35]

$$t_{\text{ex}} = 2\pi^2 \nu_z C \sqrt{L_{\text{ion}} L_{\text{Ca}^+}}, \tag{9}$$

where C is the total capacitance defined above, L_{ion} and L_{Ca^+} are the inductances of the equivalent circuit for the ion of interest and the Ca^+ ion, respectively. These inductances are given in generic form by

$$L = m(z_0/\alpha q)^2, \tag{10}$$

where m is the mass of the ion, z_0 is the distance from the trap center to the electrode in the axial direction (as shown in Fig. 1), α is a factor for correction due to the trap geometry (≈ 0.8), and q the electric charge. The other degrees of freedom can be cooled by sideband coupling at the sum and difference frequencies of the respective eigenfrequencies. For a trap capacity of 1 pF, a trap dimension of $z_0 = 0.5$ mm, and an axial frequency of 100 kHz, the time for cooling via coupling to the laser-cooled ion will be 8 s. This time is exactly t_{ex}, the time to exchange the amplitudes of the measurement ion and the sensor ion, as given in (9) [35]. The sensor ion is laser cooled and, if the laser is ON, its amplitude will not increase, only the amplitude of the ion of interest will be reduced. Faster cooling time can be achieved if the ion under study has a higher charge state.

Table 1 Time for cooling and/or energy exchange (t_{ex}) for different ion pairs calculated according to (9). $z_0 = 0.5$ mm, $C = 1$ pF, and $\nu_z = 100$ kHz. For further discussions see text

Ion-pair	t_{ex} (s)	$\Delta\nu_z$ (mHz)	Applied DC voltage (mV)	ΔV_{DC} (mV)
$^{1}H^{+}$–$^{40}Ca^{+}$	1.3	380	8.2	1.9×10^{-7}
$^{40}Ca^{+}$–$^{40}Ca^{+}$	8	62	328	4.0×10^{-7}
$^{187}Re^{+}$–$^{40}Ca^{+}$	17	29	1532	8.9×10^{-7}
$^{270}Db^{+}$–$^{40}Ca^{+}$	20	24	2048	9.8×10^{-7}

Table 1 shows the time to exchange the amplitudes of the ion of interest and the sensor ion t_{ex} for different ion pairs following (9). The corresponding amplitude of the DC voltage, frequency width and the required stability of the DC power supply are also shown. Note that the stability of the power supply must be very high in order to exchange the energy between the two ions. Currently, there are power supplies which fulfill this requirement, for example Ref. [36].

It is important to mention that t_{ex} depends quadratically on z_0 as can be inferred from (9) and (10). In the calculations presented here, $z_0 = 0.5$ mm which is small compared with the MPIK/UW-PTMS ($z_0 = 2.29$ mm) or with the MIT-PTMS at FSU ($z_0 = 6$ mm). The small size is not a problem provided that the ratio z/z_0 needed for the measurement using the *quantum sensor* is smaller than the one in the experiments using electronic detection. The limit to reduce further the trap size will be given by the ratio z/z_0.

The analytical solution of the coupled differential equations of the two ions, each of them represented by a capacitor and an inductance, has been given in Ref. [35]. Figure 3 shows the simulated evolution of the amplitude of the sensor ion and the ion of interest after they are coupled. The initial amplitude for the sensor ion is 1 µm while that for the ion of interest is 50 µm corresponding to a ratio $z/z_0 = 0.1$. Note that in this process no additional heating has been taken into account. Recent studies of heating rates due to stochastic field fluctuations at the electrodes or by collisions have been presented in Ref. [37] (experiment) and in Ref. [38] (theoretical model), indicating that, for a $^{25}Mg^{+}$ ion, the heating rate after Doppler cooling and switching OFF the laser beam is about 650 quanta/s. Thus, after 8 s the axial energy will be about 2 µeV which is still below the expected energy gain. Furthermore, these experiments were performed in a Paul trap and not in a Penning trap where an RF driving field is absent.

3.2 Laser cooling of the sensor ion

Laser cooling of the sensor ion in one dimension can be achieved by directing a laser beam in one direction. The other degrees of freedom can be cooled by side-band coupling [39]. After energy transfer from the ion of interest to the sensor ion (only axial direction is considered), the latter is cooled again. Here, a laser beam with sharp focus on the center of the sensor-ion trap is proposed for cooling. Focalization to a very small spot is possible by using a microscope objective. There are microscope objectives for the wavelength interval from 355 to 532 nm with a numerical aperture of 0.23, which can provide a spot size as small as 2 µm (at $\lambda = 397$ nm). With such spot size, the laser beam interacts with the sensor ion only when this crosses the center of the trap. The force due to the laser field on an ion can be represented by (see e.g. [40])

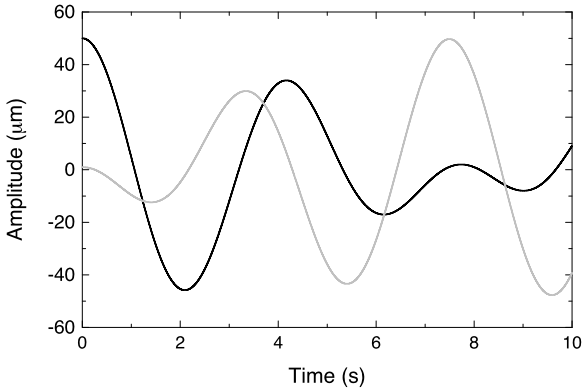

Fig. 3 Evolution of the amplitude of the sensor ion (*light grey curve*) and the ion of interest (*black curve*) versus time after they are coupled in the axial direction. The sensor ion has been laser cooled ($z \approx 1$ µm at $t = 0$) while the ion of interest moves with an axial oscillation amplitude of 50 µm. For both ions the initial conditions are: maximum amplitude and zero velocity. The common frequency is 100 kHz ($= \nu_z$) and the frequency exchange is $1/(2t_{ex})$. By changing the initial conditions to solve the equations, the evolution of the amplitude can be observed for different phases

$$\mathbf{F} = \hbar \mathbf{k} R, \tag{11}$$

where $\hbar\mathbf{k}$ is the momentum transfer from the photon to the ion, and R is the scattering rate given by

$$R = \Gamma \cdot \frac{s/2}{1 + s + (2\delta_{\text{eff}}/\Gamma)^2}. \tag{12}$$

Here Γ is the decay rate of the cooling transition, δ_{eff} is the effective laser detuning given by $\delta_{\text{eff}} = \omega - \omega_0 - \mathbf{k} \cdot \mathbf{v}$, and s is the saturation parameter

$$s = \frac{I_0}{I_{\text{sat}}} \tag{13}$$

with

$$I_{\text{sat}} = \frac{hc\pi\Gamma}{3\lambda^3}. \tag{14}$$

The equation of motion for the axial direction

$$\ddot{z} + \omega_z^2 z = \frac{F(z, \dot{z})}{m} \tag{15}$$

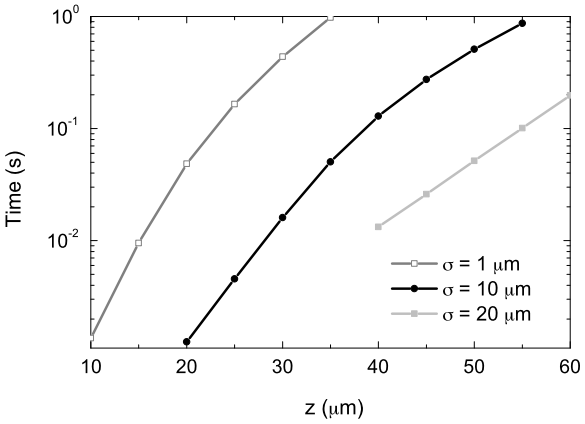

Fig. 4 Time needed to reduce the oscillation amplitude of a $^{40}Ca^{+}$ ion to that of the waist of the laser beam versus initial amplitude along z. Equation (16) has been solved numerically using a fourth-order Runge–Kutta method. For these calculations the following parameters were used: $s = 140$ (corresponding to $I_0 = 10$ mW/mm^2 and $I_{\text{sat}} = 68$ μW/mm^2), $m = 40$, $d = 1$ mm, $\nu_z = 100$ kHz and $\Delta = \Gamma/2$

(where $F(z, \dot{z})$ is the force taking into account the dependence on z due the Gaussian profile of the laser beam ($f(z) = e^{z^2/2\sigma^2}$) [41] and the dependence on the velocity $\dot{z}$ by the term δ_{eff}) results in

$$\ddot{z} + \omega_z^2 z = \frac{\Gamma}{2m} \cdot \frac{s \cdot e^{z^2/2\sigma^2}}{1 + s \cdot e^{z^2/2\sigma^2} + (2(\Delta - k\dot{z})/\Gamma)^2}. \quad (16)$$

This equation has been solved numerically using a fourth-order Runge–Kutta method. The results of the time needed to reduce the amplitude of the ion motion to be within the waist of the laser beam around the center of the trap are shown in Fig. 4 for different diameters of the laser beam ($\sigma = 1$, 10 and 20 μm). In order to obtain these results, **k** has been considered in the same direction as **v** while in the real case (Fig. 2) there should be an angle very close to 90° and therefore $\mathbf{kv} = kv\cos\alpha$. Including this angle into the calculations, the time to decrease the amplitude of the oscillation of the ion motion to that of the beam waist is expected to be larger. Once the oscillation amplitude of the ion is within the beam waist, the maximum fluorescence will be observed within a few milliseconds. The time from t_0 (laser ON) to t (maximum fluorescence) will vary depending on the initial ion oscillation amplitude and therefore on the initial ion energy.

Considering that the cooling transition in $^{40}Ca^{+}$ has a decay rate of $\Gamma = 20.7$ MHz, a number of approximately 10^8 photons/s is expected. About 10^4 photons/s will be observed due to the detection solid angle and the quantum efficiency of the photomultiplier or CCD camera. Within a time interval for the observation of the fluorescence of about 10 ms, 100 photons can be detected. The resolution in amplitude of the axial motion is better than 5 μm as shown in Fig. 4. Table 2 shows the time for several initial axial oscillation amplitudes presented in Fig. 4 together with their corresponding kinetic energies and cyclotron radii. As shown in the table, very small amplitudes in the cyclotron motion are already sufficient to observe different times which result in better resolution (compared to the axial motion). Furthermore, the small amplitude ratio z/z_0 will ensure that the ion of interest will not move far from the trap center and will be less affected by trap imperfections.

Table 2 Time needed to reduce the oscillation amplitude of a $^{40}Ca^{+}$ ion to the waist of the laser beam for different initial amplitudes z. The laser beam has a Gaussian profile ($\sigma = 10$ μm). The ratio z/z_0 considering $z_0 = 0.5$ mm, the kinetic energy for the ion and the corresponding cyclotron radius considering a 7 T magnetic field, are also listed. For this magnetic field strength, $\nu_c = 2684046.36$ Hz and $\nu_+ = 2682182.19$ Hz

z_0 (μm)	z/z_0	r_+ (μm)	E (meV)	Time (ms)
20	0.04	0.8	0.03	1.3
25	0.05	1.0	0.05	4.6
30	0.06	1.2	0.07	16.1
35	0.07	1.3	0.1	50.4
40	0.08	1.5	0.13	129
45	0.09	1.7	0.17	274
50	0.1	1.9	0.2	511
55	0.11	2.1	0.25	870

This method of measuring time to reach the maximum fluorescence becomes more sensitive in terms of detection compared with a measurement of the Doppler shift used for ion clouds by scanning a laser below resonance (see e.g. [42] and references therein). In the latter case, many ions are stored simultaneously in the trap and the number of detected photons is several orders of magnitude larger. This will allow the measurement of the fluorescence distribution and obtaining the ion cloud temperature. For a single ion one can observe the fluorescence after cooling (10^4 photons per second are expected to be detected) and get the final temperature of the ion but this temperature will be the same regardless the initial ion energy. The information it can be used is also the measurement of the time it takes to reach the maximum fluorescence. If the ion beam does not have a strong focus, this time will be shorter compared to the case proposed in this paper. However, the resolution in reach can be experimentally investigated using different intensities of the laser-cooling beam.

An improvement of the sensitivity obtained using the method proposed in this paper relies on the possibility to reduce further the energy of the sensor ion by cooling below the Doppler limit. This might be possible by using a standing wave pattern generated with two laser beams propagating in opposite directions orthogonally polarized with respect to each other. The way to generate such beams will be similar to the way used in magneto-optical traps but now only

one direction is needed. This cooling has been proposed already for ions [43]. The method does not require additional lasers and therefore can be easily implemented within the proposed setup.

3.3 Principle of mass measurement with the sensor ion

In order to determine the mass of the ion using conventional techniques, the ion must gain energy from either a quadrupole field with $\nu_{RF} = \nu_c$ (TOF technique) or from a dipole field with $\nu_{RF} = \nu_+$ (induced image-current technique). This energy gain must be now detected through the sensor ion in step 5 of the measurement procedure (Fig. 2). The detection, as explained in the previous section will be based on the measurement of the time needed by the sensor ion to be laser cooled after it has undergone energy exchange with the ion of interest.

A single mass measurement is carried out by sweeping the frequency around ν_c or ν_+. Therefore the steps from 3 to 6 in Fig. 2 must be repeated around ν_c or ν_+ in order to obtain the linewidth of the resonance. Excitation, conversion to axial motion, and energy transfer from the ion of interest to the sensor ion originates an increase of the axial oscillation amplitude of the sensor ion. This amplitude will be larger at $\nu_{RF} = \nu_c$ (quadrupolar excitation) or $\nu_{RF} = \nu_+$ (dipolar excitation) and this will be detected, since time as shown in Fig. 4, will be longer. This time for a $^{40}Ca^+$ ion in a 7 T magnetic field was listed for several radial energies in Table 2. For quadrupole excitation, the radial kinetic energy varies around ν_c [22]. For dipole excitation, the relative variation in ν_z also depends on the radial kinetic energy [25]. The detection of an electronic current or by using a micro-channel plate detector is now substituted by a measurement of the cooling time of the sensor ion after this has gained energy from the ion of interest previously excited.

4 Choice of $^{40}Ca^+$ as sensor ion

The ion used in the sensor trap should have a simple level scheme with optical transitions easily accessible by commercially available laser systems. Furthermore, it should have a mass not too light in order to avoid the operation at high harmonics. The $^{40}Ca^+$ ion is here a good compromise: It is of middle mass, avoids, as even-even nucleus, the complication of very many hyperfine Zeeman levels, and requires cw lasers which are readily available easy-to-handle diode lasers. The calcium ion has been studied extensively for quantum computation [44] and frequency standard development [45] in a Paul trap by the Innsbruck group of R. Blatt, for development of a frequency standard [46] by a group at Osaka University (also using a Paul trap), and, in a Penning trap, also for quantum information processing and ion crystallization [39] by R.C. Thompson et al. at Imperial College, London. It is important to underline that these experiments are more complicated since they need to perform side-band cooling using the transition $4^2S_{1/2} \rightarrow 3^2D_{5/2}$ (≈ 1 s half-life) at $\lambda = 729$ nm after Doppler cooling, which is the only cooling mechanism proposed for the quantum sensor. The used of a standing wave pattern mentioned in Sect. 3.2 does not require extra lasers.

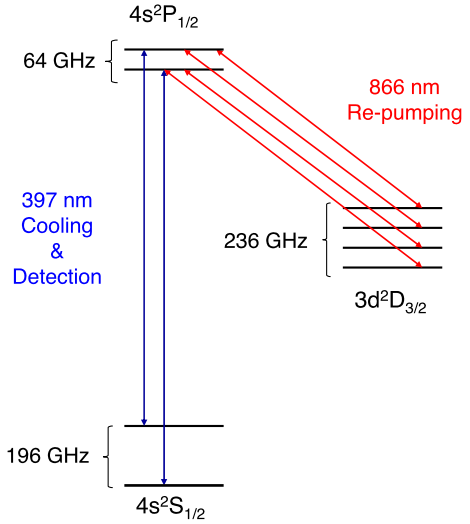

Fig. 5 Atomic level of a Ca^+ ion in a 7 T magnetic field. Only the levels needed for Doppler cooling are shown. See text for further details

The level scheme of Ca^+ for Doppler cooling in a 7 T magnetic field is shown in Fig. 5. Investigations carried out by the group at Imperial College have shown electron shelving induced due to the magnetic field. They have observed spontaneous decay from $4p^2P_{1/2} \rightarrow 3d^2D_{5/2}$ with a branching ratio relative to the decay $4p^2P_{1/2} \rightarrow 2s^2S_{1/2}$ of $4.2 \times 10^{-7}\ B^2$ (B given in Tesla) [47]. For the proposed magnetic field of 7 T, this becomes significant and therefore a re-pumping laser at $\lambda = 854$ nm is needed. Furthermore due to the Zeeman splitting up to six more frequencies have to be generated around this transition.

5 Planned pilot setup at the University of Granada

Cooling an ion in one trap by coupling this motion to a laser-cooled ion in a second trap has not been realized up to now. From the calculations presented in Ref. [35] and in this paper, this cooling scheme seems feasible. The setup proposed to be realized at the University of Granada is shown in Fig. 6. It should enable to perform the mass measurements on the ^{187}Re–^{187}Os pair at Granada and to allow the preparation of the mass measurements planned on superheavy elements at GSI. It consists of the following four main components:

1. An ion source to deliver the ions of an isotope such as rhenium or osmium, as pure ion beam. For this purpose,

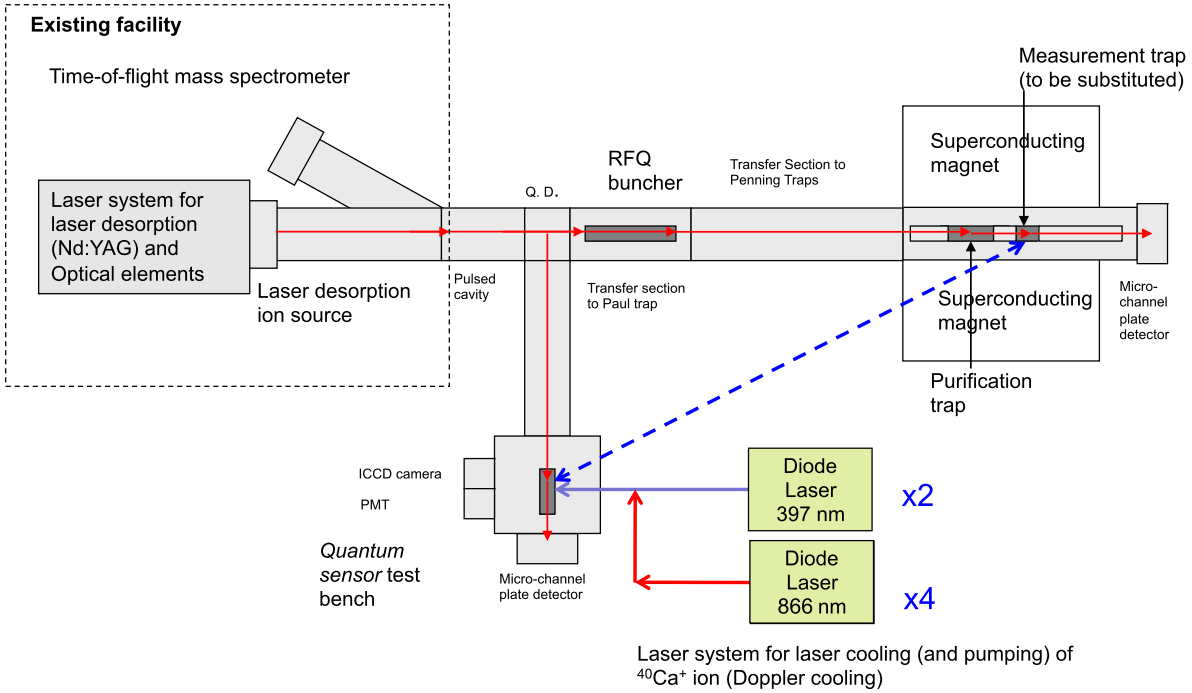

Fig. 6 Sketch of the quantum sensor setup for highly sensitive and extremely accurate mass measurements as planned at the University of Granada

we will use a system already operational at the University of Granada [48]. It consists of a Nd:YAG laser for laser desorption and ionization, a time-of-flight mass spectrometer, and ion detectors.

2. A Penning trap mass spectrometer. The planned mass spectrometer is very similar to SHIPTRAP realized some time ago by the author and co-workers at GSI [49]. Using the time-of-flight technique [22] SHIPTRAP has been successfully applied since its construction to measure the masses of many isotopes up to those of lawrencium [10]. It comprises a linear He-gas-filled radiofrequency quadrupole (RFQ) cooler and buncher [50] for accumulation, cooling and bunched ejection of the ions delivered by the ion source and a superconducting solenoid housing two Penning traps, a so-called *purification trap* for isobaric separation of the injected ion bunch and a so-called *measurement trap* which allows for isomeric separation and the mass measurement [51]. Note that blueprints from the SHIPTRAP facility are already available [52] and that mass measurements with 10^{-8} accuracy can be performed at Granada on stable isotopes immediately after duplicating the GSI system and applying the TOF technique. The superconducting magnet will be identical to the one used at SHIPTRAP. This device produces two homogeneous magnetic field regions: an area with 1 ppm/cm^3 homogeneity for the *purification trap* and another one with 0.1 ppm/cm^3 for the *measurement trap*. This trap will later be substituted by the *quantum sensor trap* once this device is tested and operational.
3. A test bench for the *quantum sensor*. It enables to study the concept of the quantum sensor (the laser-cooling process and the detection scheme by fluorescence) independent from building up, testing and performing TOF mass measurements by use of the Penning traps. This prototype of the quantum sensor will be operated as Paul trap. The test bench will also serve to study the heating of the stored ion after switching OFF the lasers. The heating rate measured under these conditions will be larger as compared to the heating rate in a Penning trap without RF field.
4. A laser system comprising two diode lasers with $\lambda = 397$ nm and $\lambda = 866$ nm which has been already delivered by the company TOPTICA (DL 100 /PRO DESIGN) including the associated equipment. When moving the quantum sensor from the test bench to the superconducting magnet (dotted line in Fig. 6), the number of lasers has to be multiplied by a factor of 2 (for the transitions at $\lambda = 397$ nm) and by a factor of 4 (for the transitions at $\lambda = 866$ nm) due to the large Zeeman splittings.

Challenges of the *quantum sensor* concept are the small dimensions of the trap system (diameter ≈ 1 mm), the stability of the applied potentials ($\approx$ 100–200 nV), and an optimized coupling of the two traps. Micromachinery will be applied and power supplies with extreme stability must be used which are commercially available [36]. The coupling of the ions through the endcaps is also challenging as they cannot be electrically floating. This can be solved by having

a large resistor to ground in parallel with a radiofrequency switch as mentioned in Sect. 3.1.

6 Planned experiments and outlook

The applicability of the quantum sensor to the measurements performed at SHIPTRAP is based on the modulation of the radial energy as a function of a radiofrequency ν_{RF} around ν_c, which is the excitation scheme using the TOF technique [22]. With the quantum sensor, however, the detection of the time-of-flight using the micro-channel plate is substituted by the measurement of the time to achieve fluorescence. Figure 7 shows the time needed to decrease the amplitude of the ion motion to that of the laser beam at the waist as a function of ν_{RF} for a Ca^+ ion in a 7 T magnetic field for two different diameters of the laser beam. The conversion from radial energy to time is done after applying a polynomial fit to the data listed in Table 2 (columns 4 and 5).

The curve in Fig. 7 can be built up using about 10 data points. For each point one needs to follow the procedure shown in Fig. 2, taking a few tens of seconds. Therefore, a complete measurement would take around ≈ 5 min which allows a comfortable investigation of the isotopes decaying by fission at the end of the α-decay chain of elements $Z = 114$, 116, and 117 [for example ^{270}Db ($T_{1/2} = 3.4$ h)] [7, 53].

The masses of ^{187}Re and ^{187}Os will be carried out also using the same system (Fig. 6). In this respect it is clear from the results shown in Fig. 7 and in Table 2 that the masses of Re and Os can be accomplished, however the relative mass uncertainty for the neutrino mass problem needs to be 2–3 orders of magnitude better than the one delivered by the TOF technique. The two possibilities previously described are the technique used by Van Dyck et al. [25] and the determination of the phase of the ion motion as pursued by Pritchard et al. [27].

The method by Van Dyck et al. is based on the measurement of $\delta\nu_z/\nu_z$ as a function of ν_+ following the equation [25]

$$\frac{\delta\nu_z}{\nu_z} = \left(\frac{B_2 d^2}{B} - 3C_4\alpha^2\right) \cdot \frac{E_c}{qU}. \tag{17}$$

Using the data in Table 2, $E_c/qU = 0.4$ for $z = 50$ µm. For the pair Ca^+–Ca^+, the axial frequency must be stable within 60 mHz in order to get coupling of the two ions. Thus for an axial frequency of about 100 kHz, $\delta\nu_z/\nu_z = 6 \times 10^{-7}$ (Table 1). In order to observe the frequency shift by observing the shortest time to get fluorescence (no coupling), the term in parentheses in (17) must be larger than 1.5×10^{-6} at $\nu_{RF} = \nu_+$. Therefore $B_2 d^2/B > 3C_4\alpha^2 + 1.5 \times 10^{-6}$. The time to observe fluorescence will be a minimum provided $C_4 < -1.2 \times 10^{-5}$. By changing the sign of C_4 one can get

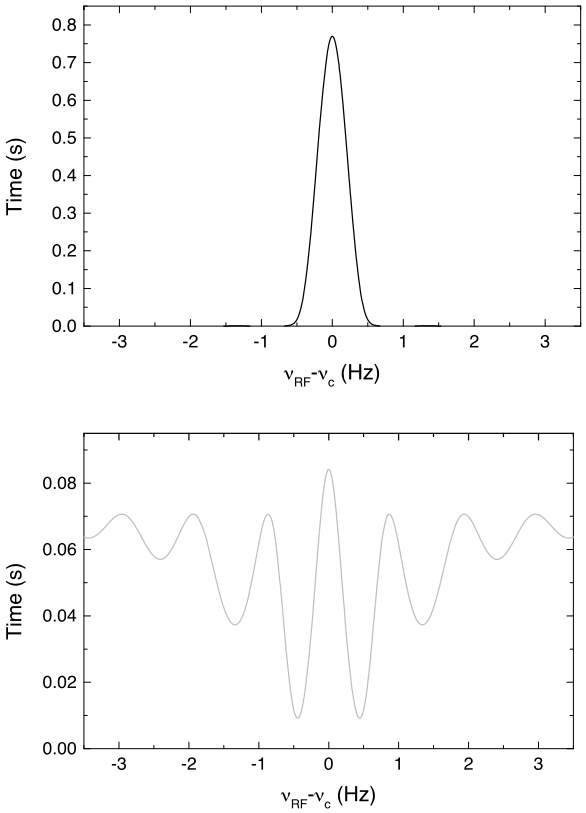

Fig. 7 Time to reduce the amplitude of the ion motion to that of the laser at the beam waist versus frequency of an applied RF field around ν_c. *Upper panel*: $\sigma = 10$ µm; *lower panel*: $\sigma = 20$ µm. The ion is Ca^+ and the magnetic field is 7 T. The maximum energy of the ion is 235 µeV (axial amplitude of 50 µm)

the curve in opposite way (for $\nu_{RF} < \nu_+$, $C_4 > 1.2 \times 10^{-5}$). This can be done using the guard rings of the measurement trap with a precision of $|C_4| \approx 10^{-5}$ [54]. The measurement in this way is expected to be highly sensitive. Note that to get 10 ppt accuracy by using (6) one needs to measure the axial frequency with less than 0.5 ppb (less than 2 mHz).

The detection of $\delta\nu_z/\nu_z$ as a function of ν_+ is affected by systematic effects which have been presented in detail in Ref. [25]. There are several systematic shifts which are depending on the energy of the ion in the trap and are expected to be reduced as this new method allows for better cooling of the ion and does need only very small radial oscillation amplitudes for detection. The other systematic shifts might depend on how well one can determine the axial and modified-cyclotron frequencies using the quantum sensor.

The method developed by Pritchard et al., of detecting the phase of the cyclotron frequency can be considered here after looking to Fig. 8, where the evolution of the amplitude of the sensor ion is shown starting the coupling at different initial phases of the ion of interest and the sensor ion. As observed from the figure, it is possible to observe differences in the temporal evolution of the amplitude due to the initial phase. In this figure the phase difference between the two

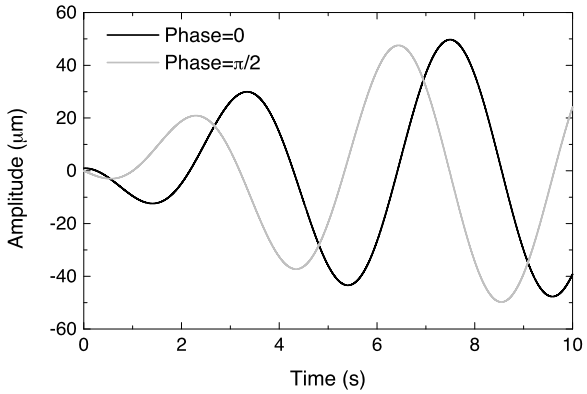

Fig. 8 Evolution of the amplitude of the sensor ion versus time after coupling to the ion of interest. The difference between the *two curves* are the initial conditions: *black*: maximum amplitude and zero velocity; *light grey*: zero amplitude and maximum velocity. The difference between the time to get the first maxima is more than 1 second

curves is $\pi/2$. This opens up new possibilities in the determination of the cyclotron frequency by detecting the phase versus evolution time and fitting the data point by a least squares method. One can fix a time than might be for example the first expected maximum of the amplitude when the initial phase is zero (maximum amplitude and zero velocity). This can be defined as the time t_0 to switch ON the laser after energy exchange for all the measurements. The time t needed to observed the maximum fluorescence will then vary with the phase of the ion motion when the ions are coupled.

Acknowledgements I want to thank especially H.-Jürgen Kluge for fruitful discussions on the concept of the quantum sensor. Many thanks go to Richard Thompson, Danny Segal and their group at the Imperial College. The time I have spent there was very important to learn about laser cooling in a Penning trap. I also want to thank Reiner Blatt, Markus Heinrich and Michael Brownutt for showing me in their lab in Innsbruck highly advanced laser systems, and finally to Michael Block, spokesman of the SHIPTRAP collaboration, who is the main responsible for the breakthroughs achieved recently at this facility opening new possibilities as for the ideas presented in this paper. This research has been partly supported by the Ramón y Cajal budget and by the projects FPA2009-14091-C02-02 and FPA2010-14803 from the Spanish Ministry of Science and Innovation. This project will be funded by the European Union with contract 278648-TRAPSENSOR obtained in the ERC-2011-StG call.

References

1. K. Blaum, Phys. Rep. **425**, 1 (2006)
2. D. Rodríguez, K. Blaum, W. Nörtershäuser, M. Ahammed, A. Algora, G. Audi, J. Äystö et al., Eur. Phys. J. ST **183**, 1 (2010)
3. S. Hofmann, G. Münzenberg, Rev. Mod. Phys. **72**, 733 (2000)
4. K. Morita, K. Morimoto, D. Kaji, T. Akiyama, S. Goto, H. Haba, E. Ideguchi, R. Kanungo, K. Katori, H. Koura, H. Kudo, T. Ohnishi, A. Ozawa, T. Suda, K. Sueki, H. Xu, T. Yamaguchi, A. Yoneda, A. Yoshida, Y. Zhao, J. Phys. Soc. Jpn. **73**, 2593 (2004)
5. Y. Oganessian, J. Phys. G, Nucl. Part. Phys. **34**, R165 (2007)
6. K. Tatsumi, J. Corish, Pure Appl. Chem. **82**, 753 (2010)
7. C. Dülmann, W. Schädel, A. Yakushev, A. Türler, K. Eberhardt, J.V. Kratz et al., Phys. Rev. Lett. **104**, 252701 (2010)
8. M. Block, D. Ackermann, K. Blaum, C. Droese, M. Dworschak, S. Eliseev, T. Fleckenstein, E. Haettner, F. Herfurth, F.P. Heßberger, S. Hofmann, J. Ketelaer, J. Ketter, H.-J. Kluge, G. Marx, M. Mazzocco, Yu.N. Novikov, W.R. Plaß, A. Popeko, S. Rahaman, D. Rodríguez, C. Scheidenberger, L. Schweikhard, P.G. Thirolf, G.K. Vorobyev, C. Weber, Nature **463**, 785 (2010)
9. M. Dworschak, M. Block, D. Arckermann, G. Audi, K. Blaum, C. Droese, S. Eliseev, T. Fleckenstein, E. Haettner, F. Herfurth, F.P. Heßberger, S. Hofmann, J. Ketelaer, J. Ketter, H.-J. Kluge, G. Marx, M. Mazzocco, Yu.N. Novikov, W.R. Plaß, A. Popeko, S. Rahaman, D. Rodríguez, C. Scheidenberger, L. Schweikhard, P.G. Thirolf, G.K. Vorobyev, M. Wang, C. Weber, Phys. Rev. C **81**, 064312 (2010)
10. E. Minaya-Ramirez, D. Arckermann, K. Blaum, M. Block, C. Droese, Ch.E. Düllmann, M. Dworschak, M. Eibach, S. Eliseev, E. Haettner, F. Herfurth, F.P. Heßberger, S. Hofmann, J. Ketelaer, G. Marx, M. Mazzocco, D. Nesterenko, Yu. Novikov, W.R. Plaß, D. Rodríguez, C. Scheidenberger, L. Schweikhard, P.G. Thirolf, C. Weber, in preparation
11. M. Schädel, Angew. Chem. Int. Ed. **45**, 368 (2006)
12. Q.R. Ahmad, R.C. Allen, T.C. Andersen, J.D. Anglin, J.C. Barton, E.W. Beier et al., Phys. Rev. Lett. **89**, 011301 (2002)
13. E.W. Otten, C. Weinheimer, Rep. Prog. Phys. **71**, 086201 (2008)
14. V.M. Lobashev, Prog. Part. Nucl. Phys. **48**, 123 (2002)
15. Ch. Kraus, B. Bornschein, L. Bornschein, J. Bonn, B. Flatt, A. Kovalik, B. Ostrick, E.W. Otten, J.P. Schall, Th. Thümmler, Ch. Weinheimer, Eur. Phys. J. C **40**, 447 (2005)
16. J. Angrik, T. Armbrust, A. Beglarian, U. Besserer, J. Blümer, J. Bonn et al., KATRIN Design Report 2004, Wissenschaftliche Berichte FZKA, 7090
17. M. Galeazzi, F. Fontanelli, F. Gatti, S. Vitale, Phys. Rev. C **63**, 014302 (2000)
18. M. Sisti, C. Arnaboldi, C. Brofferio, G. Ceruti, O. Cremonesi, E. Fiorini, A. Giuliani, B. Margesin, L. Martensson, A. Nuccioti, M. Pavan, G. Pessina, S. Pirro, E. Previtali, L. Soma, M. Zen, Nucl. Instrum. Methods A **520**, 125 (2004)
19. A. Monfardini, C. Arnaboldi, C. Brofferio, S. Capelli, F. Capozzi, O. Cremonesi, C. Enss, E. Fiorini, A. Fleischmann, L. Foggetta, G. Gallinaro, L. Gastaldo, F. Gatti, A. Giuliani, P. Gorla, R. Kelley, C.A. Kilbourne, B. Margesin, D. McCammon, C. Nones, A. Nucciotti, M. Pavan, M. Pedretti, D. Pergolesi, G. Pessina, F.S. Porter, M. Prest, E. Previtali, P. Repetto, M. Ribeiro-Gomez, S. Sangiorgio, M. Sisti, Nucl. Instrum. Methods A **559**, 346 (2006)
20. http://mare.dfm.uninsubria.it/frontend/exec.php
21. L.S. Brown, G. Gabrielse, Rev. Mod. Phys. **58**, 233 (1986)
22. M. König, G. Bollen, H.-J. Kluge, T. Otto, J. Szerypo, Int. J. Mass Spectrom. **142**, 95 (1995)
23. M. Comisarow, J. Chem. Phys. **69**, 4097 (1978)
24. A.G. Marshall, C.L. Hendrickson, G.S. Jackson, Mass Spectrom. Rev. **17** (1998)
25. R.S. Van Dyck Jr., D.B. Pinegar, S. Van Liew, S.L. Zafonte, Int. J. Mass Spectrom. **251**, 231 (2006)
26. H.-J. Kluge, Hyperfine Interact. **196**, 295 (2010)
27. S. Rainville, J.K. Thompson, D.E. Pritchard, Science **303**, 334 (2004)
28. M. Redshaw, J. McDaniel, E.G. Myers, Phys. Rev. Lett. **100**, 093002 (2008)
29. G. Gabrielse, Int. J. Mass Spectrom. **251**, 273 (2006)
30. E.A. Cornell, R.M. Weisskoff, K.R. Boyce, R.W. Flanagan Jr., G.P. Lafyatis, D.E. Pritchard, Phys. Rev. Lett. **63**, 1674 (1989)
31. E.A. Cornell, R.M. Weisskoff, K.R. Boyce, D.E. Pritchard, Phys. Rev. A **41**, 312 (1990)
32. E.A. Cornell, PhD Thesis, Massachusetts Institute of Technology, 1990

33. J. Ketelaer, K. Blaum, M. Block, K. Eberhardt, M. Eibach, R. Ferrer, S. George, F. Herfurth, J. Ketter, Sz. Nagy, Eur. Phys. J. A **42**, 311 (2009)
34. R.M. Weisskoff, G.P. Lafyatis, K.R. Boyce, E.A. Cornell, R.W. Flanagan, D.E. Pritchard, J. Appl. Phys. **63**, 4599 (1988)
35. D.J. Heinzen, D.J. Wineland, Phys. Rev. A **42**, 2977 (1990)
36. http://www.stahl-electronics.com/
37. R.J. Epstein, S. Seidelin, D. Leibfried, J.H. Wesenberg, J.J. Bollinger, J.M. Amini, R.B. Blakestad, J. Britton, J.P. Home, W.M. Itano, J.D. Jost, E. Knill, C. Langer, R. Ozeri, N. Shiga, D.J. Wineland, Phys. Rev. A **76**, 033411 (2007)
38. J.H. Wesenberg, R.J. Epstein, D. Leibfried, R.B. Blakestad, J. Britton, J.P. Home, W.M. Itano, J.D. Jost, E. Knill, C. Langer, R. Ozeri, S. Seidelin, D.J. Wineland, Phys. Rev. A **76**, 053416 (2007)
39. D.R. Crick, H. Ohadi, I. Bhatti, R.C. Thompson, D.M. Segal, Opt. Express **16**, 2351 (2008)
40. D. Leibfried, R. Blatt, C. Monroe, D. Wineland, Rev. Mod. Phys. **75**, 281 (2003)
41. R.C. Thompson, J. Papadimitriou, J. Phys. B, At. Mol. Opt. Phys. **33**, 3393 (2000)
42. M.A. van Eijkelenborg, M.E.M. Storkey, D.M. Segal, R.C. Thompson, Phys. Rev. A **60**, 3903 (1999)
43. D.J. Wineland, J. Dalibard, C. Cohen-Tannoudji, J. Opt. Soc. Am. B **9**, 32 (1992)
44. F. Splatt, M. Harlander, M. Brownnutt, F. Zähringer, R. Blatt, W. Hänsel, New J. Phys. **11**, 103008 (2009)
45. M. Chwalla, J. Benhelm, K. Kim, G. Kirchmair, T. Monz, M. Riebe, P. Schindler, A.S. Villar, W. Hänsel, C.F. Roos, R. Blatt, M. Abgrall, G. Santarelli, G.D. Rovera, Ph. Laurent, Phys. Rev. Lett. **102**, 023002 (2009)
46. K. Matsubara, K. Hayasaka, Y. Li, H. Ito, S. Nagano, M. Kajita, M. Hosokawa, Appl. Phys. Express **1**, 067011 (2008)
47. D.R. Crick, S. Donnellan, D.M. Segal, R.C. Thompson, Phys. Rev. A **81**, 052503 (2010)
48. D. Rodríguez, V. Sonnenschein, K. Blaum, M. Block, H.-J. Kluge, A.M. Lallena, S. Raeder, K. Wendt, Rev. Sci. Instrum. **81**, 013301 (2010)
49. M. Block, D. Ackermann, D. Beck, K. Blaum, M. Breitenfeldt, A. Chauduri, A. Doemer, S. Eliseev, D. Habs, S. Heinz, F. Herfurth, F.P. Hessberger, S. Hofmann, H. Geissel, H.-J. Kluge, V. Kolhinen, G. Marx, J.B. Neumayr, M. Mukherjee, M. Petrick, W. Plass, W. Quint, S. Rahaman, C. Rauth, D. Rodríguez, C. Scheidenberger, L. Schweikhard, M. Suhonen, P.G. Thirolf, Z. Wang, C. Weber (the SHIPTRAP Collaboration), Eur. Phys. J. A **25**, 49 (2005)
50. D. Rodríguez, PhD thesis. University of Valencia, 2003
51. S. Rahaman, M. Block, D. Ackermann, D. Beck, A. Chaudhuri, S. Eliseev, H. Geissel, D. Habs, F. Herfurth, F.P. Heßberger, S. Hofmann, G. Marx, M. Mukherjee, J.B. Neumayr, M. Petrick, W. Plaß, W. Quint, C. Rauth, D. Rodríguez, C. Scheidenberger, L. Schweikhard, P.G. Thirolf, C. Weber, Int. J. Mass Spectrom. **251**, 146 (2006)
52. M. Block, private communication
53. Yu.Ts. Oganessian, F.Sh. Abdullin, P.D. Bailey, D.E. Benker, M.E. Bennett, S.N. Dmitriev, J.G. Ezold, J.H. Hamilton, R.A. Henderson, M.G. Itkis, Yu.V. Lobanov, A.N. Mezentsev, K.J. Moody, S.L. Nelson, A.N. Polyakov, C.E. Porter, A.V. Ramayya, F.D. Riley, J.B. Roberto, M.A. Ryabinin, K.P. Rykaczewski, R.N. Sagaidak, D.A. Shaughnessy, I.V. Shirokovsky, M.A. Stoyer, V.G. Subbotin, R. Sudowe, A.M. Sukhov, Yu.S. Tsyganov, V.K. Utyonkov, A.A. Voinov, G.K. Vostokin, P.A. Wilk, Phys. Rev. Lett. **104**, 142502 (2010)
54. G. Gabrielse, Phys. Rev. A **27**, 2277 (1983)